# Depth-resolved subcycle dynamics of photoionization in solids

P. A. Zhokhov[1,2] and A. M. Zheltikov[1,2,3,4]

[1]*Department of Physics and Astronomy, Texas A&M University, College Station, Texas 77843, USA*

[2]*Russian Quantum Center, 143025 Skolkovo, Moscow Region, Russia*

[3]*Physics Department, International Laser Center, M.V. Lomonosov Moscow State University, 119992 Moscow, Russia*

[4]*Kazan Quantum Center, A.N. Tupolev Kazan National Research Technical University, 420126 Kazan, Russia*

(Received 22 May 2017; published 21 September 2017)

We develop a theoretical framework for the analysis of ultrafast dynamics of photoionization in solids that treats the electron density buildup resolved within the field cycle jointly with the propagation dynamics of the laser driver. We show that while the standard, cycle-averaging photoionization models predict a monotonic buildup of the electron density within the driver pulse, the cycle-resolved photoionization model used in this work reveals a subcycle modulation of optical properties of a solid, giving rise to complex patterns of reflected and transmitted fields and providing a source for optical harmonic generation. Propagation effects are shown to heavily distort the spectra of high-order harmonics. Still, the analysis of harmonic spectra and the temporal structure of the harmonic field reveals physically significant properties of the nonlinear-optical response, suggesting the existence of attosecond bursts of interband optical-harmonic emission.

DOI: 10.1103/PhysRevA.96.033415

## I. INTRODUCTION

Photoionization in solids has been a subject of in-depth research since the invention of lasers. This process is central to understanding a broad class of laser-solid interaction effects, including laser-induced breakdown [1–3], laser filamentation [4,5], laser micromachining [6,7], and, since recently, high-order harmonic generation in solids [8–19] and attosecond spectroscopy of band-gap dynamics [20]. Although many of the fundamental properties of solids, including first and foremost, a higher atomic density and the band structure of electron energy states, are different from those of gases, photoionization in solids has much in common with the physics of photoionization in gas media. The universal physics behind photoionization is highlighted by the Keldysh theory of photoionization, which was developed simultaneously for gases and solids in Keldysh's seminal 1964 paper [21].

Analysis of photoionization effects in solids inevitably starts with a calculation of the photoionization rate, that is, the rate of electron transitions from the valence to the conduction band. The Keldysh theory of photoionization [21] provides the key to understanding the behavior of the photoionization rate of solids as a function of laser intensity, laser frequency, and band gap of a solid. Over five decades, this theory has been pivotal to the research in laser science, providing a commonly accepted framework for a quantitative analysis of photoionization in a remarkable diversity of light-matter interaction phenomena, including laser-induced breakdown [1], high-order harmonic [22] and terahertz [23] generation, as well as filamentation of ultrashort light pulses [4,5,24]. The Keldysh formalism, however, involves averaging over the field cycle as a part of photoionization rate derivation. As a result, it offers no recipe for understanding photoionization dynamics within the field cycle or calculating the rate of photoionization by ultrashort, broadband laser field waveforms. In a recent work [25], the Keldysh theory of photoionization of solids has been extended to include photoionization by arbitrarily short driving pulses with an arbitrary pulse shape.

Analysis of photoionization in the bulk of a solid is, however, in no way reducible to photoionization rate calculation. Photoionization gives rise to an ultrafast buildup of the electron density, which translates into a rapid modulation of optical properties through ionization-induced radiation loss and intensity-dependent changes in the refractive index [26–28]. As a result, photoionization dynamics becomes strongly coupled to the propagation dynamics of the laser driver.

Here, we develop a theoretical framework for the analysis of ultrafast dynamics of photoionization in solids that treats the field-cycle-resolved buildup of the electron density jointly with the propagation dynamics of the laser driver, which probes the ionization-induced modulation of the optical properties of the material. Analysis performed with the use of this model reveals unusual, often unexpected, ultrafast laser-matter interaction effects in a rapidly ionizing solid. At high field intensities, ionization-induced ultrafast modulation of the optical properties of a solid is shown to strongly couple the dynamics of photoionization to the propagation of the laser driver.

## II. PHOTOIONIZATION AND ULTRAFAST OPTICAL RESPONSE OF A SOLID: ANALYTICAL FRAMEWORK

The main goal of this section is to develop an analytical framework for the analysis of the ultrafast optical response of a rapidly ionizing solid to an ultrashort laser pulse. To this end, we examine the polarization $\vec{P}(t)$ and the current density $\vec{J}(t)$ induced in a medium by a laser field $\vec{E}(t)$,

$$P_i(t) = \int_{-\infty}^{t} \chi_{ij}(t,t')E_j(t')dt', \tag{1}$$

$$J_i(t) = \int_{-\infty}^{t} \sigma_{ij}(t,t')E_j(t')dt'. \tag{2}$$

Here, $\chi_{ij}(t,t')$ is the optical susceptibility, $\sigma_{ij}(t,t')$ is the conductivity, and the subscripts $i,j$ stand for the Cartesian coordinates, $i,j = x,y,z$.

 

Since the polarization can be expressed through the current density,

$$\vec{J}(t) = \frac{d\vec{P}(t)}{dt}, \tag{3}$$

leading to

$$\sigma_{ij}(t,t') = \frac{\partial \chi_{ij}(t,t')}{\partial t} + \chi_{ij}(t,t)\delta(t-t'), \tag{4}$$

where $\delta(\tau)$ is the Dirac delta function, choosing between $\vec{P}(t)$ and $\vec{J}(t)$ is often a matter of convenience. In a canonical treatment [29,30], the optical response of bound electrons is analyzed in terms of polarization $\vec{P}(t)$, while the current density $\vec{J}(t)$ would be a natural choice for a characterization of the optical response of free, or for that matter, conduction-band electrons.

In our model, we treat the optical response of a solid in a standard two-band approximation [31,32], searching for the solution for the electron wave function in the form of a superposition

$$|\psi(t)\rangle = \sum_{\vec{k}} V(\vec{k},t)|v,\vec{k}\rangle + C(\vec{k},t)|c,\vec{k}\rangle, \tag{5}$$

where $|v,\vec{k}\rangle$ and $|c,\vec{k}\rangle$ are the Bloch-wave state vectors with a quasimomentum $\vec{k}$ in the valence and conduction bands, respectively.

With the expansion coefficients $C(\vec{k},t)$ and $V(\vec{k},t)$ found from the relevant time-dependent Schrödinger equation, we calculate the photoionization probability $\rho(t)$ and the photoionization current density $\vec{J}(t)$. It is convenient and physically meaningful to represent the current density $\vec{J}(t)$ as the sum $\vec{J}(t) = \vec{J}^{(i)}(t) + \vec{J}^{(c)}(t)$, where the terms $\vec{J}^{(i)}(t)$ and $\vec{J}^{(c)}(t)$ relate to the inter- and intraband parts of the overall current density. Physically, the $\vec{J}^{(c)}(t)$ term describes the current of electrons or holes driven by the field within the respective bands of a semiconductor, while $\vec{J}^{(i)}(t)$ represents the current induced by interband processes, including transitions of electrons from the valence to the conduction band, as well as electron-hole recombination [8,9,12].

We consider a periodic dispersion profile, consistent with the nearest-neighbor interaction approximation [33],

$$\mathcal{E}(\vec{p}) = \mathcal{E}_g + \Delta - \frac{\Delta}{D}\sum_{j=1}^{D}\cos(p_j d_j), \tag{6}$$

where $D$ is the number of spatial dimensions, $\Delta$ is the band width, and $d_j$ is the lattice constant in the direction $j$.

Calculation details are presented in the Appendix. The physical scope of our analysis and the overall scheme of our calculations are as follows. We present the electron wave function in the form of Eq. (5) and plug this wave function into the time-dependent Schrödinger equation with the Hamiltonian as defined by Eq. (A3) in the Appendix. This Hamiltonian treats a semiconductor or a dielectric in a standard two-band approximation [31,32] and includes the external field in the dipole approximation. The time-dependent Schrödinger equation leads to a set of coupled partial differential equations for the expansion coefficients $C(\vec{k},t)$ and $V(\vec{k},t)$ in Eq. (5) [Eq. (A5) in the Appendix]. Solving these equations and defining the pertinent probability amplitudes in Eq. (A9), we then calculate the field-induced polarization [Eqs. (A15) and (A17)] and photocurrent [Eqs. (A19), (A20), and (A24)]. In the regime where the population of the conduction band remains much smaller than the population of the valence band, we also derive an explicit expression for the ionization rate [Eq. (A37)]. With the dispersion profile taken in the form of Eq. (6), this leads us to Eqs. (A60)–(A64) for $\rho(t)$, $\vec{J}^{(i)}(t)$, and $\vec{J}^{(c)}(t)$, which we reproduce also here for the sake of convenience,

$$\rho(t) = |\mathcal{N}|^2 \int_{-\infty}^{t}\int_{-\infty}^{t} dt_1 dt_2 \vec{E}(t_1)\cdot\vec{E}(t_2) e^{i(\mathcal{E}_g+\Delta)(t_2-t_1)} \prod_{j=1}^{D} J_0(|\Phi_j(t_2,t_1)|), \tag{7}$$

$$J_j^{(i)}(t) = 2|\mathcal{N}|^2 \int_{-\infty}^{t} dt_1 E_j(t_1)\mathrm{Re}\, e^{i(\mathcal{E}_g+\Delta)(t-t_1)} \left[\prod_{l=1}^{D} J_0(|\Phi_l(t,t_1)|)(\mathcal{E}_g+\Delta) - \frac{i\Delta}{D}\sum_{k=1}^{D} J_1(|\Phi_k(t,t_1)|)\cos[d_k A_k(t) - \arg\Phi_k(t,t_1)]\prod_{l\neq k} J_0(|\Phi_l(t,t_1)|)\right], \tag{8}$$

$$J_j^{(c)}(t) = |\mathcal{N}|^2 \int_{-\infty}^{t}\int_{-\infty}^{t} dt_1 dt_2 \vec{E}(t_1)\cdot\vec{E}(t_2) e^{i(\mathcal{E}_g+\Delta)(t_2-t_1)} \times \frac{i\Delta}{D} J_1(|\Phi_j(t_2,t_1)|)\sin[d_j A_j(t) - \arg\Phi_j(t_2,t_1)]\prod_{k\neq j} J_0(|\Phi_k(t_2,t_1)|), \tag{9}$$

where $\mathcal{E}_g$ is the band gap, $|\mathcal{N}|^2$ is the normalization factor, $J_0(z)$ and $J_1(z)$ are the zeroth- and first-order Bessel functions of the first kind, $\vec{A}(t) = \int_{-\infty}^{t}\vec{E}(t')dt'$ is the vector potential, and

$$\Phi_j(t_1,t_2) = \frac{\Delta}{D}\int_{t_1}^{t_2} e^{id_j A_j(t')}dt', \tag{10}$$

and the system of units where $\hbar = |e| = 1$ is used.

Equation (7) for the ionization probability is fully consistent with the result of Ref. [25]. It will be referred to hereinafter as the field-cycle-resolved photoionization theory (FCRPI). In accordance with their definitions [Eqs. (1) and (2)], the interband optical susceptibility and the inter- and intraband conductivities are thus given by

$$\chi_{ij}^{(i)}(t,t')=2\delta_{ij}|\mathcal{N}|^2\left[\sin[(\mathcal{E}_g+\Delta)(t-t')]\prod_{k=1}^{D}J_0(|\Phi_k(t,t')|)\right], \tag{11}$$

$$\sigma_{ij}^{(c)}(t,t') = 2|\mathcal{N}|^2\int_{-\infty}^{t'}dt_1\,E_j(t_1)\sin[(\mathcal{E}_g+\Delta)(t'-t_1)]\prod_{k\neq i}J_0(|\Phi_k(t',t_1)|)\frac{\Delta}{D}J_1(|\Phi_i(t',t_1)|)\sin[d_iA_i(t)-\arg\Phi_i(t',t_1)], \tag{12}$$

and

$$\sigma_{ij}^{(i)}(t,t') = 2\delta_{ij}|\mathcal{N}|^2\left[\cos[(\mathcal{E}_g+\Delta)(t-t')]\prod_{k=1}^{D}J_0(|\Phi_k(t,t')|)(\mathcal{E}_g+\Delta)-\frac{\Delta}{D}\sin[(\mathcal{E}_g+\Delta)(t-t')]\right.$$
$$\left.\times\sum_{k=1}^{D}J_1(|\Phi_k(t,t')|)\cos[d_kA_k(t)-\arg\Phi_k(t,t')]\prod_{l\neq k}J_0(|\Phi_l(t,t')|)\right]. \tag{13}$$

In the limiting case of $|\vec{E}|\to 0$, Eqs. (12) and (11) become, respectively,

$$\sigma_{ij}^{(c)}(t,t')\to 0, \tag{14}$$
$$\chi_{ij}^{(i)}(t,t')\to\overline{\chi}_{ij}^{(i)}(t-t'), \tag{15}$$

where

$$\overline{\chi}_{ij}^{(i)}(\tau) = 2\delta_{ij}|\mathcal{N}|^2\sin[(\mathcal{E}_g+\Delta)\tau]J_0\left(\frac{\Delta}{D}\tau\right)^D \tag{16}$$

Fourier transform of Eq. (16) yields a frequency-domain optical susceptibility,

$$\hat{\chi}_{ij}^{(i)}(\omega) = \delta_{ij}|\mathcal{N}|^2\frac{D}{\Delta}\left[\mathcal{F}_D^0(\mathcal{E}_+)+\mathcal{F}_D^0(\mathcal{E}_-)\right], \tag{17}$$

where $\mathcal{E}_\pm=\frac{\mathcal{E}_g+\Delta\pm\omega}{\Delta}$, and

$$\mathcal{F}_D^n(x) = \int_0^\infty ie^{-ixz}J_0\left(\frac{z}{D}\right)^{D-n}J_1\left(\frac{z}{D}\right)^n\frac{dz}{z^n}. \tag{18}$$

The functions $\mathcal{F}_1^0$ and $\mathcal{F}_2^0$ can be found in an analytical form,

$$\mathcal{F}_1^0(x) = (x^2-1)^{-1/2}, \tag{19}$$

and

$$\mathcal{F}_2^0(x) = \frac{2}{\pi}\frac{K(x^{-2})}{x}, \tag{20}$$

where $K(x)$ is the complete elliptic integral of the first kind.

As an important example, we consider zinc oxide ($\mathcal{E}_g=3.3$ eV, $\Delta/D=2.5$ eV, and $d_i=2.8$ A) irradiated by pulses with a central wavelength $\lambda_0=3.25\ \mu$m, which corresponds to a frequency $\omega_0=0.12\mathcal{E}_g$. Electron-hole pairs gain an energy equal to the band gap over one lattice period when driven by the field $E^0=\frac{\mathcal{E}_g}{ed_i}\approx 1.14$ V/A. At $\lambda_0=3.25\ \mu$m, a linearly polarized field with such an amplitude corresponds to a field intensity $I^0=\frac{(E^0)^2}{2n(\lambda_0)}\sqrt{\frac{\mu_0}{\epsilon_0}}=9$ TW/cm$^2$, where $n(\lambda_0)\approx 1.9$ is the refractive index, $\mu_0=(4\pi)^{-1}\times 10^{-7}$ H/m and $\epsilon_0=8.85\times 10^{-12}$ F/m are, respectively, the vacuum permeability and the vacuum permittivity.

To find the normalization factor $|\mathcal{N}|^2$, we compare the results of Eqs. (11)– (20) with the available experimental data [34] for the dielectric function $\epsilon(\omega)=1+4\pi\hat{\chi}(\omega)$ (Fig. 1). Remarkably, when the normalization factor $|\mathcal{N}|^2$ defined from this comparison is plugged into Eq. (7), we achieve a very close agreement between the predictions of our model and the Keldysh theory of photoionization [21] within its region of applicability (Fig. 2). Thus, with a single value of $|\mathcal{N}|^2$, Eqs. (11)–(20) provide a reasonably accurate fit for both the available experimental data for the dielectric function of a representative semiconductor and the predictions of the Keldysh theory of photoionization.

## III. NUMERICAL ANALYSIS

Analytical expressions for the polarization and current density of a rapidly ionizing solid derived in the previous section are central to a numerical analysis of spatiotemporal dynamics of ultrashort pulses in such materials, because they provide closed-form expressions that can be used to define source terms in numerical schemes integrating Maxwell equations. Below in the paper, we show how this analytical model can be integrated into a finite-difference time-domain (FDTD) analysis [35,36], enabling a depth-resolved study of ultrafast photoionization in solids. The FDTD method provides a powerful tool for a direct numerical integration of Maxwell equations for electric and magnetic fields, helping to analyze a broad class of analytically unsolvable problems, including those dealing with complex scenarios of radar signal propagation [37–39], properties of optical fields on the nanoscale [40–43], plasmonic field enhancement [44–47], and subcycle pulse generation in resonant media [48,49].

In our version, the standard FDTD scheme is modified to include the polarization and current density of a fast-ionizing solid, as derived in Sec. II. We consider a laser pulse that propagates along the $z$ axis, in the direction of positive for $z$, along the normal to the interface between a solid and a vacuum, located at $z=0$. Polarization of the electric field is chosen along one of the crystallographic directions, with the field-induced photocurrents driven in the same direction. Propagation of such a pulse inside a solid is analyzed by numerically integrating the coupled equations for

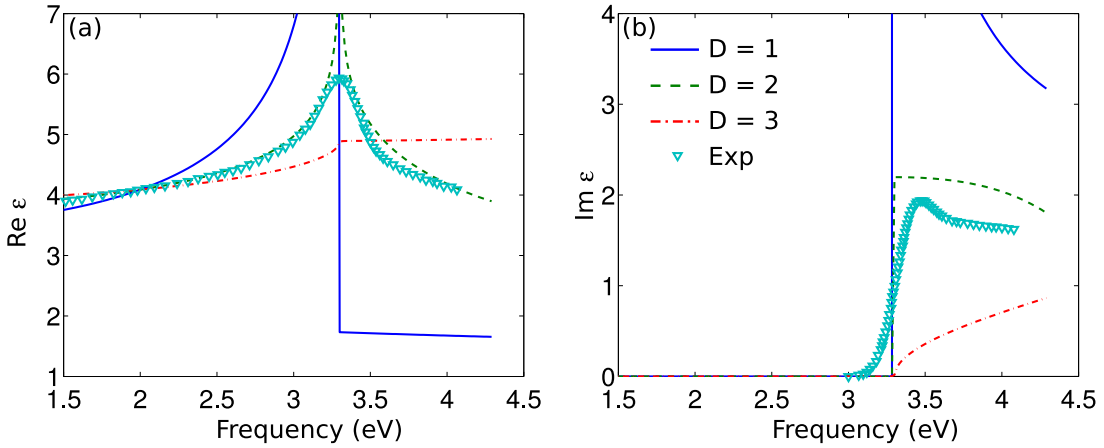


FIG. 1. (a) Real and (b) imaginary parts of the dielectric function $\epsilon(\omega)$ calculated as a function of the photon energy using Eq. (17) for parameters of ZnO with $D = 1$ (solid blue line), $D = 2$ (dashed green line), and $D = 3$ (dash-dotted red line). The available experimental data [34] are shown by cyan triangles.

the $x$ component of the electric displacement $D_x$ and the $y$ component of the magnetic field $H_y$,

$$\frac{1}{c}\frac{\partial D_x}{\partial t} = \frac{\partial H_y}{\partial z} - 4\pi J_x, \tag{21}$$

$$\frac{1}{c}\frac{\partial H_y}{\partial t} = \frac{\partial D_x}{\partial z} - 4\pi \frac{\partial P_x}{\partial z}. \tag{22}$$

Here $D_x = E_x + 4\pi P_x$, $E_x$ is the $x$ component of the electric field, $P_x$ is the $x$ component of polarization, $J_x$ is the $x$ component of the current, and $c$ is the speed of light in vacuum. The vacuum-dielectric interface lies in the $xy$ plane.

At the $n$th step of the FDTD procedure along the time variable, the values of $D_x$ and $H_y$ found at the previous step, $D_j^n$ and $H_{j+1/2}^n$, are used to define the current values of these fields, $D_j^{n+1}$ and $H_{j+1/2}^{n+1/2}$, according to the following scheme:

$$D_j^{n+1} = D_j^n + \frac{c\Delta t}{\Delta z}\left(H_{j+1/2}^{n+1/2} - H_{j-1/2}^{n+1/2}\right) - 4\pi c\Delta t J_j^{(c),n}, \tag{23}$$

$$H_{j+1/2}^{n+1/2} = H_{j+1/2}^n + \frac{c\Delta t}{\Delta z}\left[D_{j+1}^n - D_j^n - 4\pi\left(P_{j+1}^n - P_j^{(t),n}\right)\right]. \tag{24}$$

Here, $j$ is the number of the step in space along the $z$ coordinate, with Cartesian indices $x$ and $y$ suppressed for brevity. Outside the solid, that is, for $z < 0$, we set $J^{(c)}(t) = P^{(i)}(t) = 0$. Inside the solid, for $z > 0$, $J_x$ and $P_x$ are calculated using the analytical expressions presented in Sec. II. Intraband transitions are included through the current density term in Eq. (21), while interband transitions are included through the polarization term in Eq. (22).

## IV. RESULTS AND DISCUSSION

Numerical analysis reveals a complex, intensity-dependent picture of nonlinear-optical interaction of an ultrashort laser pulse with a rapidly ionizing solid (Figs. 3–5), in which photoionization is strongly coupled to propagation effects. Unlike the canonical, Keldysh-type models of photoionization, which enable calculation of only cycle-averaged

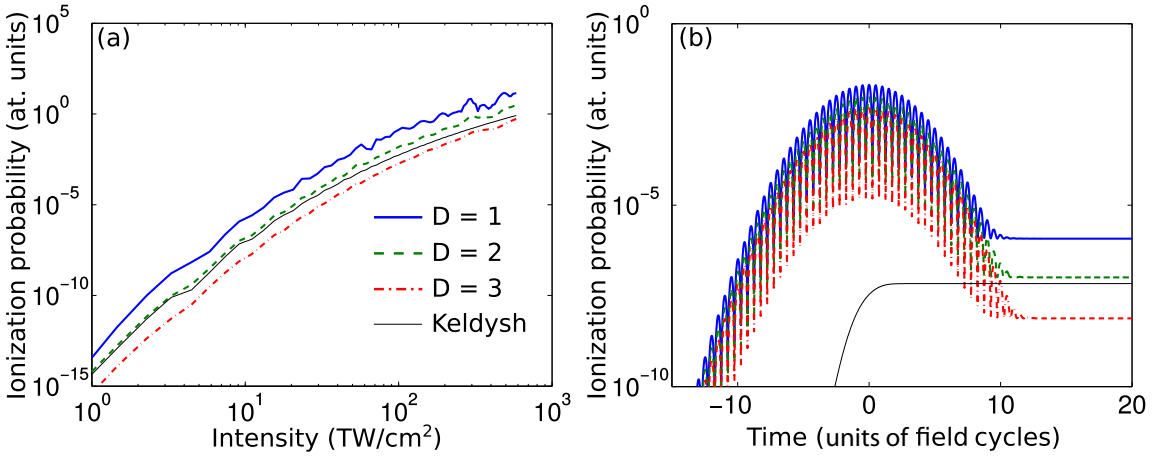


FIG. 2. (a) Ionization probability as a function of the laser intensity and (b) time for a peak intensity of 9 TW/cm$^2$ calculated for parameters of ZnO with the use of 1D FCRPI (solid blue line), 2D FCRPI (dashed green line), 3D FCRPI (dash-dotted red line), and the Keldysh model [21] (thin solid black line). The central wavelength of the laser pulse is 3.25 $\mu$m and the FWHM pulse width is 5 field cycles.

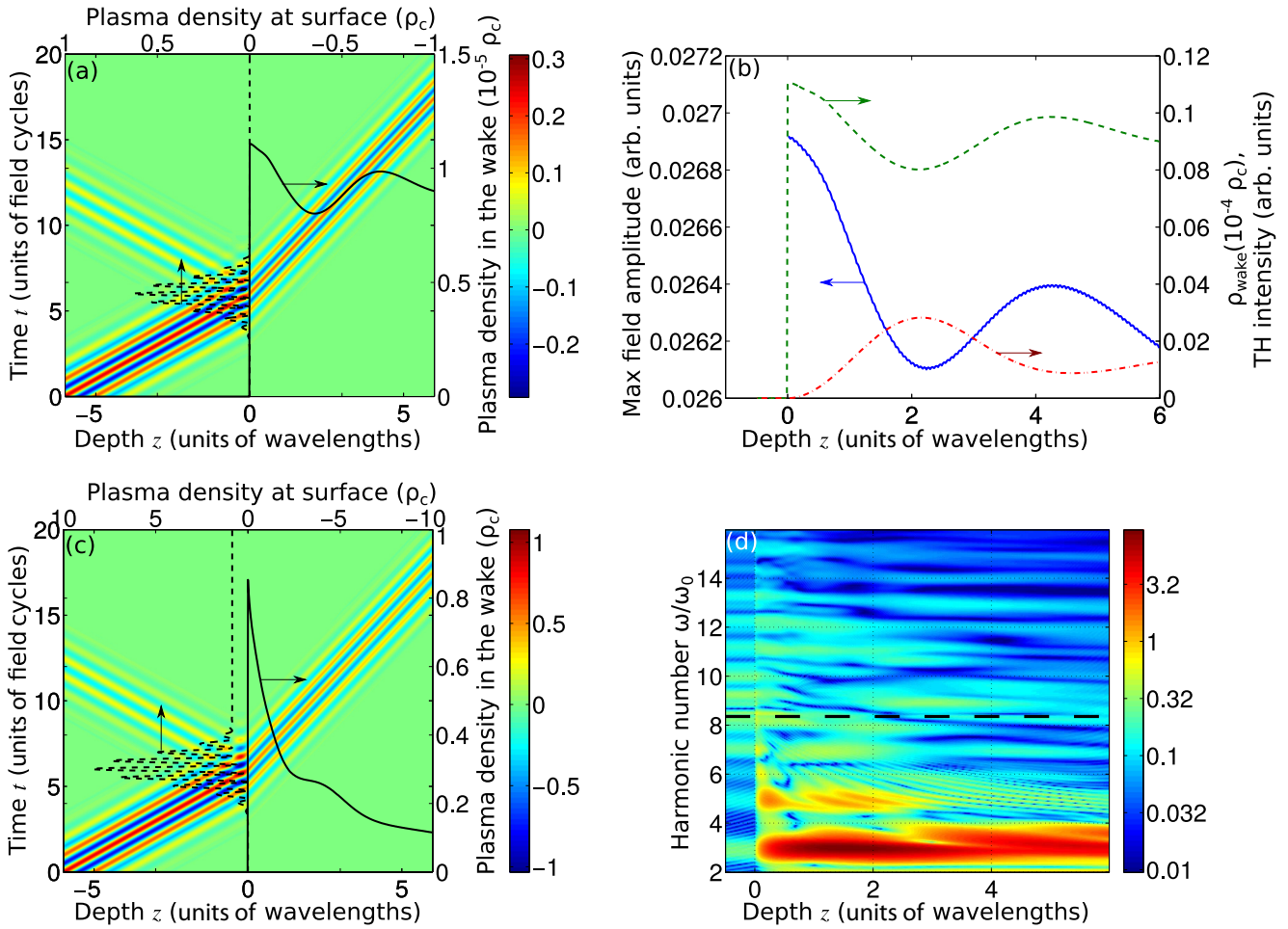


FIG. 3. (a, c) The field as a function of time $t$ (in field cycles) and propagation coordinate $z$ (in units of $\lambda_0$) near the vacuum-solid interface. The laser pulse propagates toward positive $z$. The vacuum-solid interface is located at $z = 0$. The dashed black line shows the electron density at the surface as a function of time. The solid black line is the plasma density in the wake of the laser pulse. (b) The maximum field amplitude (blue curve), the electron density in the wake of the pulse (dashed green curve), and the third-harmonic intensity (red dash-dotted curve) as functions of $z$. (d) The spectrum of the field as a function of $z$ and the harmonic number. The black dash-dotted line shows the band-gap frequency. The input laser intensity is 1 TW/cm$^2$ (a, b) and 12 TW/cm$^2$ (c, d). The central wavelength of the laser pulse is 3.25 $\mu$m. Material parameters are those of ZnO.

photoionization rates, our model of photoionization resolves the ultrafast dynamics of photoelectron currents within the field cycle. This dynamics, as our analysis shows (Figs. 3–5), gives rise to other, often unexpected, ultrafast laser-matter interaction effects in a rapidly ionizing solid.

While the Keldysh-type models of photoionization predict a monotonic buildup of the electron density from the leading edge of the pulse to its trailing edge [Fig. 2(b)], the cycle-resolved model of photoionization used in this paper reveals an oscillatory dynamics of the photoionization rate and photoelectron currents, in which oscillations of $\rho(t)$ and $J(t)$ follow the cycles of the driver field. This oscillatory dynamics translates into a subcycle modulation of the reflection, refraction, and ionization-induced loss, giving rise to complex patterns of reflected and transmitted fields [Figs. 3(f), 3(c) 4(a), and 4(b)] and providing a source for optical harmonic generation both in reflection [$z < 0$ in Figs. 3(d), 4(c) and 4(d)] and transmission [$z > 0$ in Figs. 3(d), 4(c) and 4(d)].

For low field intensities [Figs. 3(a) and 3(b)], the harmonic spectrum of the nonlinear-optical response is dominated by the third harmonic. Since the third harmonic is strongly phase-mismatched relative to the driver field, third-harmonic generation is confined to a short length on the order of the driver wavelength [Fig. 3(b)]. Beyond this length, the energy of the third harmonic transfers back to the driver field. As a result, the intensity of the driver field displays a well-resolved minimum within $\sim\lambda_0$ from the surface, followed by a local maximum, giving rise to a nonmonotonic behavior of the electron density as a function of $z$ [Figs. 3(a) and 3(b)].

Laser pulses with higher field intensities tend to generate much higher electron densities and much stronger photoelectron currents [Fig. 3(c)], which radically enhances ionization-induced reflection and refraction [Figs. 3(c), 4(a) and 4(b)]. Laser pulses with higher intensities also give rise to more efficient high-order harmonic generation [Figs. 3(d), 4(c) 4(d), and 5(a)]. Reflected harmonics are clearly seen in Figs. 4(c) and 4(d) as well-resolved horizontal stripes, reflecting their

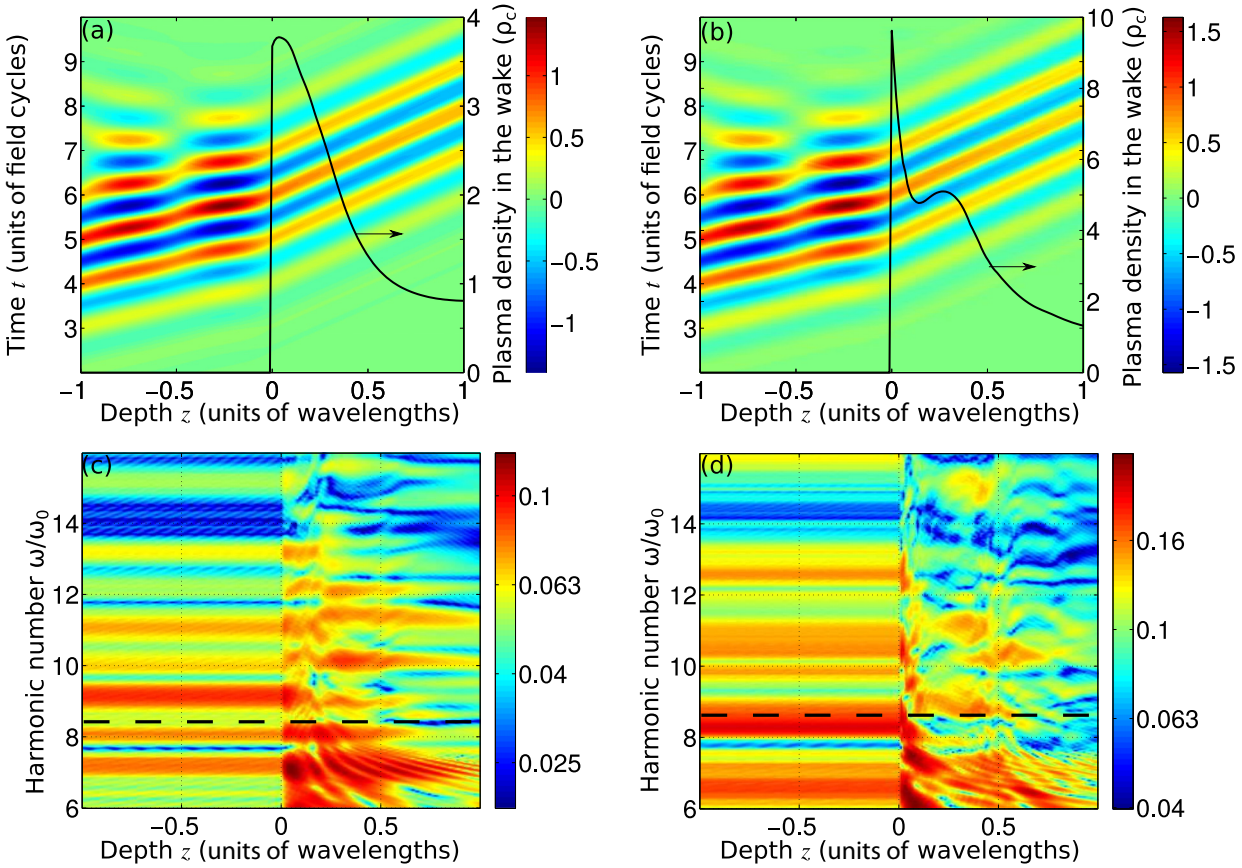


FIG. 4. (a, b) The field as a function of time $t$ (in field cycles) and propagation coordinate $z$ (in units of $\lambda_0$) near the vacuum-solid interface with the plasma density in the wake of the laser pulse shown by the solid black line. (c, d) The spectra of the field as a function of $z$ and the harmonic number. The input laser intensity is 20 TW/cm$^2$ (a, c) and 25 TW/cm$^2$ (b, d). The central wavelength of the laser pulse is 3.25 $\mu$m. Material parameters are those of ZnO.

purely linear propagation in the regime of $z < 0$, that is, in vacuum. Optical harmonics generated in transmission [$z > 0$ in Figs. 3(d), 4(c) and 4(d)] continue to exchange energy with the driver field, as well as with each other as they propagate inside the solid. This entire cascade of energy transfer processes is largely controlled by phase matching. However, because of a rapidly varying refraction and dispersion induced by ultrafast ionization, the buildup of each individual harmonic is drastically different from the canonical fringe patterns, observed for optical harmonics generated in a stationary, uniform medium.

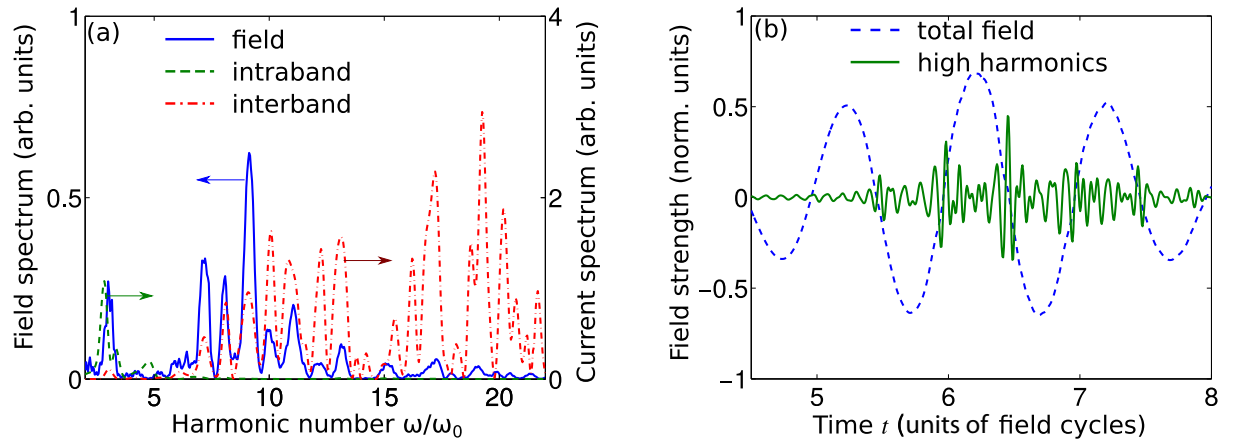


FIG. 5. (a) The spectra of the reflected field (solid blue line), the intraband current (dashed green line), and the interband current (dash-dotted red line). (b) The total field (dashed blue line) and the field of high harmonics with frequencies above the band gap (solid green line) at $z = 0.1\lambda_0$. The input laser intensity is 20 TW/cm$^2$. The central wavelength of the laser pulse is 3.25 $\mu$m. Material parameters are those of ZnO.

Thus, the propagation effects combined with an ultrafast ionization-induced modulation of dielectric properties of a solid heavily distort the spectra of high-order harmonics [Figs. 3(d), 4(c) 4(d), and 5(a)]. The map between harmonic spectra and the electron band structure of a solid, which is often the goal that high-harmonic generation experiments in solids pursue [8,17,18], is very hard to decipher in this regime. Still, even in this parameter space, the analysis of harmonic spectra [Fig. 5(a)] and the temporal structure of the harmonic field [Fig. 5(b)] reveals an important relation between the intra- and interband mechanisms of optical harmonic generation. The intraband dynamics of electron wave packets driven by the laser field is seen to dominate low-order harmonic generation [the third and fifth harmonics in Fig. 5(a)]. Around the seventh harmonic, the contributions of the intra- and interband mechanisms are comparable.

For harmonics lying above the band gap of the material [shown by the dashed vertical line in Figs. 3(d), 4(c) and 4(d)], the interband mechanism dominates over the intraband processes. At the first stage of interband harmonic generation, an electron is transferred from the valence band to the conduction band through nonlinear photoionization, leaving behind a hole in the conduction band. This electron then recombines with the hole, emitting a high-frequency photon. Since this process involves a transition of an electron from the valence to the conduction band as its first stage, interband harmonics become especially intense between the central part of the few-cycle laser driver and its trailing edge [Fig. 5(b)]. Moreover, as can be readily seen from Fig. 5(b), the interband harmonics are mainly emitted within extremely short, subfemtosecond time intervals around the instants of time when the field is zero and the magnitude of the vector potential is at its maximum. Such attosecond bursts of high-harmonic emission are clearly seen in Fig. 5(b) for $t \approx 5.5T_0$, $6.0T_0$, $6.5T_0$, $7.0T_0$, and $7.5T_0$, $T_0$ being the field cycle.

## V. CONCLUSION

To summarize, we have developed a theoretical framework for the analysis of ultrafast dynamics of photoionization in solids that treats the field-cycle-resolved buildup of the electron density as a result of photoionization jointly with the propagation dynamics of the laser driver, which probes an ultrafast ionization-induced modulation of optical properties of the material. Analysis performed with the use of this model reveals often unexpected ultrafast laser-matter interaction effects in a rapidly ionizing solid. At high field intensities, refraction and loss induced by ultrafast ionization are shown to strongly couple the dynamics of photoionization to the propagation of the laser driver. We show that while the standard, cycle-averaging photoionization models predict a monotonic buildup of the electron density within the driver pulse, the cycle-resolved photoionization model used in this work reveals a subcycle modulation of optical properties of a solid, giving rise to complex patterns of reflected and transmitted fields and providing a source for optical harmonic generation. Propagation effects are shown to heavily distort the spectra of high-order harmonics. Still, the analysis of harmonic spectra and the temporal structure of the harmonic field reveals physically significant properties of the nonlinear-optical response, suggesting the existence of attosecond bursts of interband optical-harmonic emission.

## ACKNOWLEDGMENTS

This research was supported in part by the Russian Foundation for Basic Research (Projects No. 17-52-53092, No. 16-52-50069, and No. 16-02-00843), the Welch Foundation (Grant No. A-1801), and ONR (Award No. 00014-16-1-2578). Research into ultrafast spectrochronography has been supported by the Russian Science Foundation (Project No. 17-12-01533). Research into waveguide systems for quantum technologies has been supported by the Government of Russian Federation (Project No. 14.Z50.31.0040).

## APPENDIX: OPTICAL RESPONSE OF A PHOTOIONIZED SOLID

We start with a field-free Hamiltonian of an electron in a solid semiconductor treated in a two-band approximation:

$$H_0 = \sum_{\vec{k}} \mathcal{E}_v(\vec{k})|v,\vec{k}\rangle\langle v,\vec{k}| + \mathcal{E}_c(\vec{k})|c,\vec{k}\rangle\langle c,\vec{k}|. \tag{A1}$$

Here, $|v,\vec{k}\rangle$ and $|v,\vec{k}\rangle$ are the electron states in the valence and conduction bands with a quasimomentum $\vec{k}$, $\mathcal{E}_v(\vec{k})$ and $\mathcal{E}_c(\vec{k})$ are the energies of electron states with a momentum $\vec{k}$ in the valence and conduction bands, the sum is over all $\vec{k}$ in the first Brillouin zone (BZ), and the system of units uses $\hbar = |e| = 1$, $e$ being the electron charge.

To identify the inter- and intraband parts of the optical response, we isolate two terms in the electron position operator $\vec{R}$. The first, intraband term is related to the motion of an electron within a band, $i\frac{\partial}{\partial\vec{k}}$. For the second, interband term, momentum conservation dictates

$$\vec{R} = \sum_{\vec{k}} \vec{X}(k)(|c,\vec{k}\rangle\langle v,\vec{k}| + |v,\vec{k}\rangle\langle c,\vec{k}|) + i\frac{\partial}{\partial\vec{k}}. \tag{A2}$$

The time-dependent Hamiltonian of an electron in the presence of the field in the dipole approximation is then given by

$$H(t) = \sum_{\vec{k}} \mathcal{E}_v(\vec{k})|v,\vec{k}\rangle\langle v,\vec{k}| + \mathcal{E}_c(\vec{k})|c,\vec{k}\rangle\langle c,\vec{k}| + \vec{E}(t)\cdot\vec{R}. \tag{A3}$$

The single-electron wave function can be written as

$$|\psi(t)\rangle = \sum_{\vec{k}} V(\vec{k},t)|v,\vec{k}\rangle + C(\vec{k},t)|c,\vec{k}\rangle. \tag{A4}$$

The time-dependent Schrödinger equation leads to the partial differential equations (PDEs) for the coefficients $C(\vec{k},t)$ and $V(\vec{k},t)$ (we omit $\vec{k},t$ arguments for brevity).

$$\begin{aligned} i\frac{\partial V}{\partial t} &= \mathcal{E}_v(\vec{k})V + \vec{E}(t)\cdot\left(\vec{X}(\vec{k})C + i\frac{\partial V}{\partial\vec{k}}\right), \\ i\frac{\partial C}{\partial t} &= \mathcal{E}_c(\vec{k})C + \vec{E}(t)\cdot\left(\vec{X}(\vec{k})V + i\frac{\partial C}{\partial\vec{k}}\right). \end{aligned} \tag{A5}$$

Since the PDEs are linear in derivatives both over time and momentum, it is possible to turn them into ordinary differential

equations (ODEs) by the method of characteristics. Namely, we introduce variable transformation

$$\begin{aligned} \vec{p} &= \vec{k} + \vec{A}(t), \\ \tilde{t} &= t, \end{aligned} \tag{A6}$$

where $\vec{A}(t) = \int_{-\infty}^{t} \vec{E}(t')dt'$ is the vector potential. The derivative transformation is then

$$\begin{aligned} \frac{\partial}{\partial \vec{k}} &= \frac{\partial}{\partial \vec{p}}, \\ \frac{\partial}{\partial t} &= \frac{\partial}{\partial \tilde{t}} + \vec{E}(t) \cdot \frac{\partial}{\partial \vec{p}}. \end{aligned} \tag{A7}$$

Equation (A5) can be thus rewritten as

$$\begin{aligned} i\frac{dV}{d\tilde{t}} &= \mathcal{E}_v(\vec{p} - \vec{A}(\tilde{t}))V + \vec{E}(\tilde{t}) \cdot \vec{X}(\vec{p} - \vec{A}(\tilde{t}))C, \\ i\frac{dC}{d\tilde{t}} &= \mathcal{E}_c(\vec{p} - \vec{A}(\tilde{t}))C + \vec{E}(\tilde{t}) \cdot \vec{X}(\vec{p} - \vec{A}(\tilde{t}))V. \end{aligned} \tag{A8}$$

Here, once again, we omit the $\vec{p}$ and $\tilde{t}$ arguments of $V$ and $C$ for brevity.

We now introduce the probability amplitudes

$$\begin{aligned} v(\vec{p},\tilde{t}) &= V(\vec{p},\tilde{t})e^{i\int_{-\infty}^{\tilde{t}} \mathcal{E}_v(\vec{p}-A(t'))dt'}, \\ c(\vec{p},\tilde{t}) &= C(\vec{p},\tilde{t})e^{i\int_{-\infty}^{\tilde{t}} \mathcal{E}_c(\vec{p}-A(t'))dt'}, \end{aligned} \tag{A9}$$

which remain time independent in the absence of the field.

These probability amplitudes can be found from the ODEs

$$\begin{aligned} i\frac{dv}{d\tilde{t}} &= \vec{E}(\tilde{t}) \cdot \vec{X}(\vec{p} - \vec{A}(\tilde{t}))ce^{-i\int_{-\infty}^{\tilde{t}} \mathcal{E}(\vec{p}-A(t'))dt'}, \\ i\frac{dc}{d\tilde{t}} &= \vec{E}(\tilde{t}) \cdot \vec{X}(\vec{p} - \vec{A}(\tilde{t}))ve^{i\int_{-\infty}^{\tilde{t}} \mathcal{E}(\vec{p}-A(t'))dt'}, \end{aligned} \tag{A10}$$

where $\mathcal{E}(\vec{p}) = \mathcal{E}_c(\vec{p}) - \mathcal{E}_v(\vec{p})$ is the electron-hole dispersion relation. The exact solution of Eq. (A10) can be written as an unwieldy time-ordered product of unitary evolution operators. Before making any further approximations, let us express the photoionization probability and the photocurrent density through $c(\vec{p},\tilde{t})$ and $v(\vec{p},\tilde{t})$. In what follows we omit the tilde above the time argument since $\tilde{t} = t$.

The quantum-mechanical expectation value of the projection operator,

$$\hat{\rho} = \sum_{k} |c,\vec{k}\rangle\langle c,\vec{k}|, \tag{A11}$$

gives the time-dependent photoionization probability

$$\rho(t) = \langle\hat{\rho}\rangle = \sum_{\vec{k}} |\vec{c}(\vec{k} + \vec{A}(t),t)|^2. \tag{A12}$$

Since the dispersion relation in the first Brillouin zone is periodic, summation in Eq. (A12) can be performed either in $\vec{k}$ or $\vec{p}$:

$$\rho(t) = \sum_{\vec{p}} |\vec{c}(\vec{p},t)|^2. \tag{A13}$$

Polarization per unit volume is then found by averaging the coordinate operator,

$$\vec{P}(t) = -\langle\vec{R}\rangle, \tag{A14}$$

where the minus sign reflects the negative electron charge. Equation (A14) yields

$$\begin{aligned} \vec{P}(t) &= \sum_{\vec{k}} \vec{X}(k)[C(\vec{k},t)^* V(\vec{k},t) + V(\vec{k},t)^* C(\vec{k},t)] \\ &\quad + i\sum_{\vec{k}} \left( C(\vec{k},t)^* \frac{\partial}{\partial \vec{k}} C(\vec{k},t) + V(\vec{k},t)^* \frac{\partial}{\partial \vec{k}} V(\vec{k},t) \right) \\ &= \sum_{\vec{p}} 2\mathrm{Re}\vec{X}(\vec{p} - \vec{A}(t))c(\vec{p},t)^* v(\vec{p},t) e^{i\int_{-\infty}^{t} \mathcal{E}(\vec{p}-\vec{A}(t'))dt'} \\ &\quad + \sum_{\vec{p}} \left( c(\vec{p},t)^* \frac{\partial c(\vec{p},t)}{\partial \vec{p}} + v(\vec{p},t)^* \frac{\partial v(\vec{p},t)}{\partial \vec{p}} \right) \\ &\quad + \sum_{\vec{p}} \left( |c(\vec{p},t)|^2 \int_{-\infty}^{t} \frac{\partial \mathcal{E}_c(\vec{p} - \vec{A}(t'))}{\partial \vec{p}} dt' + |v(\vec{p},t)|^2 \right. \\ &\quad \left. \times \int_{-\infty}^{t} \frac{\partial \mathcal{E}_v(\vec{p} - \vec{A}(t'))}{\partial \vec{p}} dt' \right). \end{aligned} \tag{A15}$$

Since $|v(\vec{p},t)|^2 = 1 - |c(\vec{p},t)|^2$ and the energy-momentum dispersion relations are periodic, we find $\sum_p \frac{\partial \mathcal{E}_v}{\partial \vec{p}} = 0$. Equation (A15) then leads to

$$\begin{aligned} \vec{P}(t) &= \sum_{\vec{p}} 2\mathrm{Re}\vec{X}(\vec{p} - \vec{A}(t))c(\vec{p},t)^* v(\vec{p},t) e^{i\int_{-\infty}^{t} \mathcal{E}(\vec{p}-\vec{A}(t'))dt'} \\ &\quad + \sum_{\vec{p}} \left( c(\vec{p},t)^* \frac{\partial c(\vec{p},t)}{\partial \vec{p}} + v(\vec{p},t)^* \frac{\partial v(\vec{p},t)}{\partial \vec{p}} \right. \\ &\quad \left. + |c(\vec{p},t)|^2 \int_{-\infty}^{t} \frac{\partial \mathcal{E}(\vec{p} - \vec{A}(t'))}{\partial \vec{p}} dt' \right). \end{aligned} \tag{A16}$$

The photocurrent density is

$$\vec{J}(t) = \frac{d\vec{P}(t)}{dt}. \tag{A17}$$

Since the expectation values of Hermitian quantum-mechanical operators, representing observable physical parameters, are independent of whether time evolution is described in the Schrödinger or the Heisenberg picture, we have

$$\vec{J} = -\frac{d\langle R\rangle}{dt} = -\left\langle \frac{dR}{dt} \right\rangle = i\langle[H(t),\vec{R}]\rangle = i\langle[H_0,\vec{R}]\rangle. \tag{A18}$$

Here, the last equality reflects the fact that $\vec{R}$ commutes with the $\vec{E}(t) \cdot \vec{R}$ term in the Hamiltonian $H(t)$. The photocurrent density is thus given by

$$\begin{aligned} \vec{J}(t) &= i\left\langle \sum_{\vec{k}} \mathcal{E}(\vec{k})\vec{X}(\vec{k})(|c,\vec{k}\rangle\langle v,\vec{k}| - |v,\vec{k}\rangle\langle c,\vec{k}|) \right\rangle \\ &\quad + i\left\langle \left[ H_0, i\frac{\partial}{\partial \vec{k}} \right] \right\rangle. \end{aligned} \tag{A19}$$

The second term in this expression,

$$\left\langle\left[H_0, i\frac{\partial}{\partial\vec{k}}\right]\right\rangle = \sum_{\vec{k}}\langle\psi(t)|[\mathcal{E}_v(\vec{k})|v,\vec{k}\rangle\langle v,\vec{k}| + \mathcal{E}_c(\vec{k})|c,\vec{k}\rangle\langle c,\vec{k}|] \times i\frac{\partial}{\partial\vec{k}}|\psi(t)\rangle - \sum_{\vec{k}}\langle\psi(t)|i\frac{\partial}{\partial\vec{k}}[\mathcal{E}_v(\vec{k})|v,\vec{k}\rangle\langle v,\vec{k}| + \mathcal{E}_c(\vec{k})|c,\vec{k}\rangle\langle c,\vec{k}|]|\psi(t)\rangle, \tag{A20}$$

can be calculated with the use of Eq. (A4):

$$\begin{aligned}\left\langle\left[H_0, i\frac{\partial}{\partial\vec{k}}\right]\right\rangle = &\sum_{\vec{k}}[\mathcal{E}_v(\vec{k})V^*(\vec{k},t)\langle v,\vec{k}| + \mathcal{E}_c(\vec{k})C^*(\vec{k},t)\langle c,\vec{k}|] \\ &\times i\frac{\partial}{\partial\vec{k}}[C(\vec{k},t)|c,\vec{k}\rangle + V(\vec{k},t)|v,\vec{k}\rangle] \\ &- \sum_{\vec{k}}[C^*(\vec{k},t)\langle c,\vec{k}| + V^*(\vec{k},t)\langle v,\vec{k}'|] \\ &\times i\left[\mathcal{E}_v(\vec{k})\frac{\partial}{\partial\vec{k}}V(\vec{k},t)|v,\vec{k}\rangle\right. \\ &\left.+\mathcal{E}_c(\vec{k})\frac{\partial}{\partial\vec{k}}C(\vec{k},t)|c,\vec{k}\rangle\right] \\ &+ \sum_{\vec{k}}|C(\vec{k},t)|^2\frac{\partial E_c(\vec{k})}{\partial\vec{k}} + |V(\vec{k},t)|^2\frac{\partial E_v(\vec{k})}{\partial\vec{k}}.\end{aligned} \tag{A21}$$

With $\langle v,\vec{k}|\frac{\partial}{\partial\vec{k}}|c,\vec{k}\rangle = \langle c,\vec{k}|\frac{\partial}{\partial\vec{k}}|v,\vec{k}\rangle = 0$, the first two terms in Eq. (A21) cancel out. Since $|V(\vec{k},t)|^2 = 1 - |C(\vec{k},t)|^2$, we find that

$$\begin{aligned}\left\langle\left[H_0, i\frac{\partial}{\partial\vec{k}}\right]\right\rangle &= i\sum_{\vec{k}}|C(\vec{k},t)|^2\frac{\partial\mathcal{E}(\vec{k})}{\partial\vec{k}} \\ &= i\sum_{\vec{p}}|c(\vec{p},t)|^2\frac{\partial\mathcal{E}(\vec{p}-\vec{A}(t))}{\partial\vec{p}}.\end{aligned} \tag{A22}$$

The expression for the photocurrent density then becomes

$$\begin{aligned}\vec{J}(t) = &\sum_{\vec{p}}2\vec{X}(\vec{p}-\vec{A}(t))\mathcal{E}(\vec{p}-\vec{A}(t)) \\ &\times \mathrm{Im}\, c(\vec{p},t)v^*(\vec{p},t)e^{-i\int_{-\infty}^{t}\mathcal{E}(\vec{p}-\vec{A}(t'))dt'} \\ &- \sum_{\vec{p}}|c(\vec{p},t)|^2\frac{\partial\mathcal{E}(\vec{p}-\vec{A}(t))}{\partial\vec{p}}.\end{aligned} \tag{A23}$$

Both the polarization and the current density can be represented as a sum of inter- and intraband components,

$$\vec{P}(t) = \vec{P}^{(i)}(t) + \vec{P}^{(c)}(t), \tag{A24}$$

$$\vec{J}(t) = \vec{J}^{(i)}(t) + \vec{J}^{(c)}(t), \tag{A25}$$

$$\vec{J}^{(i)}(t) = \frac{dP^{(i)}}{dt}, \tag{A26}$$

$$\vec{J}^{(c)}(t) = \frac{dP^{(c)}}{dt}, \tag{A27}$$

where the superscripts $(i)$ and $(c)$ denote inter- and intraband parts, respectively, and

$$P^{(i)}(t) = \sum_{\vec{p}}2\mathrm{Re}\vec{X}(\vec{p}-\vec{A}(t))c(\vec{p},t)^*v(\vec{p},t)e^{i\int_{-\infty}^{t}\mathcal{E}(\vec{p}-\vec{A}(t'))dt'}, \tag{A28}$$

$$P^{(c)}(t) = \sum_{\vec{p}}\left(c(\vec{p},t)^*\frac{\partial c(\vec{p},t)}{\partial\vec{p}} + v(\vec{p},t)^*\frac{\partial v(\vec{p},t)}{\partial\vec{p}} + |c(\vec{p},t)|^2\int_{-\infty}^{t}\frac{\partial\mathcal{E}(\vec{p}-\vec{A}(t'))}{\partial\vec{p}}dt'\right), \tag{A29}$$

$$\vec{J}^{(i)}(t) = \sum_{\vec{p}}2\vec{X}(\vec{p}-\vec{A}(t))\mathcal{E}(\vec{p}-\vec{A}(t))\mathrm{Im}\, c(\vec{p},t)v^*(\vec{p},t) \times e^{-i\int_{-\infty}^{t}\mathcal{E}(\vec{p}-\vec{A}(t'))dt'}, \tag{A30}$$

$$\vec{J}^{(c)}(t) = -\sum_{\vec{p}}|c(\vec{p},t)|^2\frac{\partial\mathcal{E}(\vec{p}-A(t))}{\partial\vec{p}}. \tag{A31}$$

Equation (A31) is very transparent and physically insightful. It describes the total intraband current as a sum over all electron momenta $\vec{p}$, with each term in this sum being a product of the electron velocity $\frac{\partial\mathcal{E}(\vec{p}-\vec{A}(t))}{\partial\vec{p}}$, conduction-band population, and the electron charge (the minus sign in front of the sum).

To verify energy conservation, we represent the ohmic loss of the field energy per unit volume at the moment of time $t$ as

$$w(t) = \int_{-\infty}^{t}\vec{E}(t')\cdot\vec{J}(t')dt' = -\int_{-\infty}^{t}\left\langle\vec{E}(t')\cdot\frac{d\vec{R}(t')}{dt'}\right\rangle dt'. \tag{A32}$$

The Heisenberg equation of motion for $\vec{R}$,

$$i\frac{d\vec{R}}{dt} = [H,\vec{R}], \tag{A33}$$

gives

$$w(t) = i\int_{-\infty}^{t}\langle[H(t'),\vec{E}(t')\cdot\vec{R}]\rangle dt'. \tag{A34}$$

Using Eqs. (A1) and (A3), we find that

$$\begin{aligned}w(t) &= i\int_{-\infty}^{t}\langle[H_0,\vec{E}(t')\cdot\vec{R}]\rangle dt' \\ &= i\int_{-\infty}^{t}\langle[H_0,H(t)]\rangle dt' \\ &= \int_{-\infty}^{t}\frac{d\langle H_0\rangle}{dt'}dt' \\ &= \langle H_0\rangle|_t - \langle H_0\rangle|_{-\infty}.\end{aligned} \tag{A35}$$

We now assume that the ionization probability is low, $|c(\vec{p},\tilde{t})| \ll |v(\vec{p},\tilde{t})|$, which is a standard approximation for the

analysis of photoionization in solids and gases [13,21,50–54]. In this regime, $v(\vec{p},\tilde{t}) \approx 1$ and the solution of Eq. (A10) gives

$$c(\vec{p},\tilde{t}) \approx -i \int_{-\infty}^{\tilde{t}} \vec{E}(t') \cdot \vec{X}(\vec{p} - \vec{A}(t')) e^{i \int_{-\infty}^{t'} \mathcal{E}(\vec{p} - \vec{A}(t''))dt''} dt'. \tag{A36}$$

A standard textbook approach [55,56] is to treat $\vec{E} \cdot X(\vec{p})$ as a quantity independent of $\vec{p}$. Since $\vec{X}(\vec{p})$ is defined by intrinsic properties of a solid, it should be field independent. Three simple vector covariant and contravariant functions [57] that can be composed out of the crystal momentum and a scalar momentum-dependent dispersion relation are

$$\vec{X}(\vec{p}) = \mathcal{N}\vec{x}_0 = \text{const}, \tag{A37}$$

$$\vec{X}(\vec{p}) = \mathcal{N}\vec{p}, \tag{A38}$$

$$\vec{X}(\vec{p}) = \mathcal{N}\frac{\partial \mathcal{E}(\vec{p})}{\partial \vec{p}} = \mathcal{N}\vec{v}(\vec{p}). \tag{A39}$$

Here, $\mathcal{N}$ is a normalization factor and the velocity $\vec{v}(\vec{p})$ is defined as $\vec{v}(\vec{p}) = \frac{\partial \mathcal{E}(\vec{p})}{\partial \vec{p}}$ with an effective electron mass as dictated by the dispersion relation $\mathcal{E}(\vec{p})$.

Equation (A39) allows a closed-form integration over the momentum space. Introducing $I(\vec{p},t,t') = I(\vec{p},t) - I(\vec{p},t')$ with

$$I(\vec{p},t) = \int_{-\infty}^{t} \mathcal{E}(\vec{p} - \vec{A}(t'))dt' \tag{A40}$$

and using Eq. (A36) for $c(\vec{p},t)$, we can write the ionization probability of Eq. (A12) and photocurrents [Eqs. (A31) and (A30)] as

$$\rho(t) = \int_{-\infty}^{t}\int_{-\infty}^{t} E_j(t_1)E_k(t_2)G_{jk}^{(\rho)}(t_1,t_2)\,dt_1\,dt_2, \tag{A41}$$

where

$$G_{jk}^{(\rho)}(t_1,t_2) = |\mathcal{N}|^2 \sum_{\vec{p}} v_j(\vec{p} - \vec{A}(t_1))v_k(\vec{p} - \vec{A}(t_2)) \times e^{iI(\vec{p},t_1) - iI(\vec{p},t_2)} \tag{A42}$$

is the photoionization cross-section tensor, $v_s$ is the $s$th component of the velocity $\vec{v}(\vec{p}) = \frac{\partial \mathcal{E}(\vec{p})}{\partial \vec{p}}$, and summation over repeated subscripts is implied.

It is straightforward to see that

$$G_{jk}^{(\rho)}(t_1,t_2) = (G_{kj}^{(\rho)}(t_2,t_1))^*. \tag{A43}$$

This leads us to

$$\rho(t) = 2\int_{-\infty}^{t} dt_1 \int_{-\infty}^{t_1} dt_2 E_j(t_1)E_k(t_2)\,\mathrm{Re}\,G_{jk}^{(\rho)}(t_1,t_2). \tag{A44}$$

In a similar manner, we find that

$$J_l^{(c)}(t) = -2\int_{-\infty}^{t} dt_1 \int_{-\infty}^{t_1} dt_2 E_j(t_1)E_k(t_2)\,\mathrm{Re}\,G_{jkl}^{(c)}(t_1,t_2,t), \tag{A45}$$

and

$$J_l^{(i)}(t) = -2\int_{-\infty}^{t} dt_1 E_j(t_1)\mathrm{Re}\,G_{jl}^{(i)}(t,t_1), \tag{A46}$$

where

$$G_{jkl}^{(c)}(t_1,t_2,t) = |\mathcal{N}|^2 \sum_{\vec{p}} e^{iI(p,t_2,t_1)} v_j(\vec{p} - \vec{A}(t_1)) \times v_k(\vec{p} - \vec{A}(t_2))v_l(\vec{p} - \vec{A}(t)), \tag{A47}$$

and

$$G_{jl}^{(i)}(t,t_1) = |\mathcal{N}|^2 \sum_{\vec{p}} e^{iI(p,t,t_1)} \mathcal{E}(\vec{p} - \vec{A}(t))v_j(\vec{p} - \vec{A}(t_1)) \times v_l(\vec{p} - \vec{A}(t)), \tag{A48}$$

with $I(\vec{p},t_2,t_1) = I(\vec{p},t_2) - I(\vec{p},t_1)$.

The interband polarization is then given by

$$P_l^{(i)}(t) = -2\int_{-\infty}^{t} dt_1 E_j(t_1)\mathrm{Im}\,G_{jl}^{(\rho)}(t,t_1). \tag{A49}$$

We choose to work in the nearest-neighbor approximation, which gives a periodic dispersion of the form

$$\mathcal{E}(\vec{p}) = \mathcal{E}_g + \Delta - \frac{\Delta}{D}\sum_{j=1}^{D} \cos(p_j d_j), \tag{A50}$$

where $D$ is the number of spatial dimensions, and $d_j$ is the lattice constant in the direction $j$.

The integral in Eq. (A40) can be taken analytically,

$$\begin{aligned} I(\vec{p},t) &= (\mathcal{E}_g + \Delta)t - \sum_{j=1}^{D} \mathrm{Re}\,\Phi_j(t)\cos p_j d_j \\ &\quad - \sum_{j=1}^{D} \mathrm{Im}\,\Phi_j(t)\sin p_j + \text{const} \\ &= (\mathcal{E}_g + \Delta)t - \sum_{j=1}^{D} |\Phi_j(t)|\cos[p_j d_j \\ &\quad - \arg\Phi_j(t)] + \text{const}, \end{aligned} \tag{A51}$$

where

$$\Phi_j(t) = \frac{\Delta}{D}\int_{-\infty}^{t} e^{iA_j(t')d_j} dt', \tag{A52}$$

and $\Phi_k(t_1,t_2) = \Phi_k(t_1) - \Phi_k(t_2)$. The constant term in Eq. (A51) depends on the choice of the zero time point and shows up only in the global phase of the wave function.

For crystals of macroscopic sizes, we have

$$\sum_{\vec{p}} \approx \frac{1}{(2\pi)^D}\int d^D\vec{p}. \tag{A53}$$

Since

$$\frac{1}{2\pi}\int_{-\pi}^{\pi} e^{ix\cos z}\cos nz\,dz = i^n J_n(z), \tag{A54}$$

and

$$\frac{1}{2\pi}\int_{-\pi}^{\pi} e^{ix\cos z}\sin nz\,dz = 0, \tag{A55}$$

for integer $n$, we find

$$\sum_{\vec{p}} v_j(\vec{p}-\vec{A}(t_1))v_k(\vec{p}-\vec{A}(t_2))e^{iI(\vec{p},t_1)-iI(\vec{p},t_2)} = \frac{\Delta^2}{2}e^{i(\mathcal{E}_g+\Delta)(t_1-t_2)}\prod_{l\neq j,k} J_0(|\Phi_l(t_1,t_2)|) \times \begin{cases} J_0(|\Phi_j(t_1,t_2)|)\cos[A_j(t_1)-A_j(t_2)] - J_2(|\Phi_j(t_1,t_2)|)\cos[A_j(t_1)+A_j(t_2)], & j=k, \\ -J_1(|\Phi_j(t_1,t_2)|)J_1(|\Phi_k(t_1,t_2)|)\sin[A_j(t_1)]\sin[A_k(t_2)], & j\neq k, \end{cases} \tag{A56}$$

where $J_n(z)$ is the Bessel function of the $n$th order.

Applying a similar procedure, we derive

$$\sum_{\vec{p}} e^{iI(\vec{p},t,t_1)}\mathcal{E}(\vec{p}-\vec{A}(t)) = e^{i(\mathcal{E}_g+\Delta)(t-t_1)}\prod_{j=1}^{D} J_0(|\Phi_j(t_2,t_1)|)(\mathcal{E}_g+\Delta) - \frac{i\Delta}{D}\sum_{j=1}^{D} e^{i(\mathcal{E}_g+\Delta)(t-t_1)}J_1(|\Phi_j(t,t_1)|)\cos[d_jA_j(t)-\arg\Phi_j(t,t_1)]\prod_{i\neq j} J_0(|\Phi_i(t,t_1)|), \tag{A57}$$

and

$$\sum_{\vec{p}} e^{iI(\vec{p},t_2,t_1)}\frac{\partial\mathcal{E}(\vec{p}-\vec{A}(t))}{\partial p_j} = -\frac{\Delta}{D}e^{i(\mathcal{E}_g+\frac{\Delta}{D})(t_2-t_1)}J_1(|\Phi_i(t_2,t_1)|)\sin[d_jA_j(t)-\arg\Phi_j(t_2,t_1)]\prod_{i\neq j} J_0(|\Phi_i(t_2,t_1)|). \tag{A58}$$

We can now write the photoionization probability and the photocurrents as

$$\rho(t) = |\mathcal{N}|^2\int_{-\infty}^{t}\int_{-\infty}^{t} dt_1dt_2\vec{E}(t_1)\cdot\vec{E}(t_2)e^{i(\mathcal{E}_g+\Delta)(t_2-t_1)}\prod_{j=1}^{D} J_0(|\Phi_j(t_2,t_1)|). \tag{A59}$$

$$J_j^{(i)}(t) = 2|\mathcal{N}|^2\int_{-\infty}^{t} dt_1E_j(t_1)\mathrm{Re}\, e^{i(\mathcal{E}_g+\Delta)(t-t_1)}\left[\prod_{l=1}^{D} J_0(|\Phi_l(t,t_1)|)(\mathcal{E}_g+\Delta) - \frac{i\Delta}{D}\sum_{k=1}^{D} J_1(|\Phi_k(t,t_1)|)\cos[d_kA_k(t)-\arg\Phi_k(t,t_1)]\prod_{l\neq k} J_0(|\Phi_l(t,t_1)|)\right], \tag{A60}$$

and

$$J_j^{(c)}(t) = |\mathcal{N}|^2\int_{-\infty}^{t}\int_{-\infty}^{t} dt_1dt_2\vec{E}(t_1)\cdot\vec{E}(t_2)e^{i(\mathcal{E}_g+\Delta)(t_2-t_1)} \times \frac{i\Delta}{D}J_1(|\Phi_j(t_2,t_1)|)\sin[d_jA_j(t)-\arg\Phi_j(t_2,t_1)]\prod_{k\neq j} J_0(|\Phi_k(t_2,t_1)|). \tag{A61}$$

This leads us to

$$\sigma_{ij}^{(c)}(t,t') = 2|\mathcal{N}|^2\int_{-\infty}^{t'} dt_1E_j(t_1)\sin[(\mathcal{E}_g+\Delta)(t'-t_1)]\prod_{k\neq i} J_0(|\Phi_k(t',t_1)|) \times \frac{\Delta}{D}J_1(|\Phi_i(t',t_1)|)\sin[d_iA_i(t)-\arg\Phi_i(t',t_1)], \tag{A62}$$

and

$$\sigma_{ij}^{(i)}(t,t') = 2\delta_{ij}|\mathcal{N}|^2\left[\cos[(\mathcal{E}_g+\Delta)(t-t')]\prod_{k=1}^{D} J_0\big(|\Phi_k(t,t')|\big)(\mathcal{E}_g+\Delta) - \frac{\Delta}{D}\sin[(\mathcal{E}_g+\Delta)(t-t')]\sum_{k=1}^{D} J_1(|\Phi_k(t,t')|)\cos[d_kA_k(t)-\arg\Phi_k(t,t')]\prod_{l\neq k} J_0\big(|\Phi_l(t,t')|\big)\right]. \tag{A63}$$

[1] E. Yablonovitch and N. Bloembergen, Phys. Rev. Lett. **29**, 907 (1972).

[2] V. N. Lugovoi and A. M. Prokhorov, Sov. Phys. Usp. **16**, 658 (1974).

[3] M. Lenzner, J. Krüger, S. Sartania, Z. Cheng, C. Spielmann, G. Mourou, W. Kautek, and F. Krausz, Phys. Rev. Lett. **80**, 4076 (1998).

[4] A. Couairon and A. Mysyrowicz, Phys. Rep. **441**, 47 (2007).

[5] L. Bergé, S. Skupin, R. Nuter, J. Kasparian, and J.-P. Wolf, Rep. Prog. Phys. **70**, 1633 (2007).

[6] D. Du, X. Liu, G. Korn, J. Squier, and G. Mourou, Appl. Phys. Lett. **64**, 3071 (1994).

[7] R. R. Gattass and E. Mazur, Nat. Photon. **2**, 219 (2008).

[8] S. Ghimire, A. D. DiChiara, E. Sistrunk, G. Ndabashimiye, U. B. Szafruga, A. Mohammad, P. Agostini, L. F. DiMauro, and D. A. Reis, Phys. Rev. A **85**, 043836 (2012).

[9] G. Vampa, T. J. Hammong, N. Thir, B. E. Schmidt, F. Lgar, C. R. McDonald, T. Brabec, and P. B. Corkum, Nature **522**, 462 (2015).

[10] T. T. Luu, M. Garg, S. Y. Kruchinin, A. Moulet, M. T. Hassan, and E. Goulielmakis, Nature **521**, 498 (2015).

[11] S. Ghimire, A. D. DiChiara, E. Sistrunk, P. Agostini, L. F. DiMauro, and D. A. Reis, Nat. Phys. **7**, 138 (2011).

[12] G. Vampa, C. R. McDonald, G. Orlando, D. D. Klug, P. B. Corkum, and T. Brabec, Phys. Rev. Lett. **113**, 073901 (2014).

[13] P. G. Hawkins and M. Y. Ivanov, Phys. Rev. A **87**, 063842 (2013).

[14] G. Vampa, C. R. McDonald, G. Orlando, P. B. Corkum, and T. Brabec, Phys. Rev. B **91**, 064302 (2015).

[15] C. R. McDonald, G. Vampa, P. B. Corkum, and T. Brabec, Phys. Rev. A **92**, 033845 (2015).

[16] P. G. Hawkins, M. Y. Ivanov, and V. S. Yakovlev, Phys. Rev. A **91**, 013405 (2015).

[17] O. Schubert, M. Hohenleutner, F. Langer, B. Urbanek, C. Lange, U. Huttner, D. Golde, T. Meier, M. Kira, S. W. Koch, and R. Huber, Nat. Photon. **8**, 119 (2014).

[18] A. A. Lanin, E. A. Stepanov, A. B. Fedotov, and Z. A. M, Optica **4**, 516 (2017).

[19] M. Garg, M. Zhan, L. T. T, H. Lakhotia, T. Klostermann, G. A, and E. Goulielmakis, Nature **538**, 359 (2016).

[20] M. Schultze, K. Ramasesha, C. D. Pemmaraju, S. A. Sato, D. Whitmore, A. Gandman, J. S. Prell, L. J. Borja, D. Prendergast, K. Yabana *et al.*, Science **346**, 1348 (2014).

[21] L. V. Keldysh, Sov. Phys. JETP **20**, 1307 (1965).

[22] P. B. Corkum, Phys. Rev. Lett. **71**, 1994 (1993).

[23] M. Tonouchi, Nat. Photon. **1**, 97 (2007).

[24] A. M. Zheltikov, J. Phys. B **50**, 092001 (2017).

[25] P. A. Zhokhov and A. M. Zheltikov, Phys. Rev. Lett. **113**, 133903 (2014).

[26] A. J. Verhoef, A. V. Mitrofanov, E. E. Serebryannikov, D. V. Kartashov, A. M. Zheltikov, and A. Baltuška, Phys. Rev. Lett. **104**, 163904 (2010).

[27] A. V. Mitrofanov, A. J. Verhoef, E. E. Serebryannikov, J. Lumeau, L. Glebov, A. M. Zheltikov, and A. Baltuška, Phys. Rev. Lett. **106**, 147401 (2011).

[28] E. E. Serebryannikov, A. J. Verhoef, A. Mitrofanov, A. Baltuška, and A. M. Zheltikov, Phys. Rev. A **80**, 053809 (2009).

[29] N. Bloembergen, *Nonlinear Optics*, 4th ed. (World Scientific, Singapore, 1996).

[30] Y. R. Shen, *The Principles of Nonilinear Optics* (Wiley-Interscience, New York, 2003).

[31] E. O. Kane, J. Phys. Chem. Solids **1**, 249 (1957).

[32] E. O. Kane, J. Appl. Phys. **32**, 83 (1961).

[33] V. L. Bonch-Bruevich and S. G. Kalaschnikov, *Halbleiterphysik* (VEB, Berlin, 1982).

[34] E. Agocs, B. Fodor, B. Pollakowski, B. Beckhoff, A. Nutsch, M. Jank, and P. Petrik, Thin Solid Films **571**, 684 (2014).

[35] K. S. Yee, IEEE Trans. Antennas Propag. **14**, 302 (1966).

[36] D. Sullivan, *Electromagnetic Simulation Using the FDTD Method*, 2nd ed. (Wiley, New York, 2013).

[37] J. M. Bourgeois and G. S. Smith, IEEE Trans. Geosci. Remote Sens. **34**, 36 (1996).

[38] L. Gürel and U. Oğuz, IEEE Trans. Geosci. Remote Sens. **38**, 1513 (2000).

[39] S. Hu, H. Chen, C. Law, Z. Shen, L. Zhu, W. Zhang, and W. Dou, IEEE Antenn. Wireless Propag. Lett. **6**, 70 (2007).

[40] C. Lee, J. Thillaigovindan, C.-C. Chen, X. T. Chen, Y.-T. Chao, S. Tao, W. Xiang, A. Yu, H. Feng, and G. Q. Lo, Appl. Phys. Lett. **93**, 113113 (2008).

[41] G. W. Burr and A. Farjadpour, in *Proceedings of the SPIE 5733, Photonic Crystal Materials and Devices III* (SPIE, New York, 2005), p. 336.

[42] *Surface Plasmon Nanophotonics*, Springer Series in Optical Sciences No. 131, edited by M. L. Brongersma and P. G. Kik (Springer, Dordrecht, 2007).

[43] Q. Wang and S.-T. Ho, IEEE Photon. J. **2**, 49 (2010).

[44] E. Ozbay, Science **311**, 189 (2006).

[45] A. Dhawan, S. J. Norton, M. D. Gerhold, and T. Vo-Dinh, Opt. Express **17**, 9688 (2009).

[46] J. Shibayama, A. Nomura, R. Ando, J. Yamauchi, and H. Nakano, IEEE J. Quantum Electron. **46**, 40 (2010).

[47] K. H. Lee, I. Ahmed, R. S. M. Goh, E. H. Khoo, E. P. Li, and T. G. G. Hung, Prog. Electromagn. Res. **116**, 441 (2011).

[48] A. V. Tarasishin, S. A. Magnitskii, V. A. Shuvaev, and A. M. Zheltikov, Opt. Express **8**, 452 (2001).

[49] A. V. Tarasishin, S. A. Magnitskii, and A. M. Zheltikov, Opt. Commun. **193**, 187 (2001).

[50] A. M. Perelomov, V. S. Popov, and M. V. Terent'ev, Sov. Phys. JETP **23**, 924 (1966).

[51] M. V. Ammosov, N. B. Delone, and V. P. Krainov, Sov. Phys. JETP **64**, 4 (1986).

[52] V. S. Popov, Phys. Usp. **47**, 855 (2004).

[53] G. L. Yudin and M. Y. Ivanov, Phys. Rev. A **64**, 013409 (2001).

[54] V. E. Gruzdev, Phys. Rev. B **75**, 205106 (2007).

[55] F. Wooten, *Optical Properties of Solids* (Academic, New York, 1972).

[56] M. S. Dresselhaus, Solid State Physics Part II: Optical Properties of Solids, Lecture Notes, MIT, 2001 (unpublished).

[57] Landau, L. D. and E. M. Lifshitz, *The Classical Theory of Fields*, 4th ed. (Butterworth-Heinemann, Oxford, 1975).